JOURNAL OF MATERIALS SCIENCE 17 (1982) 2514–2524

Plastic deformation and fracture of notched specimens due to bending in glassy polymers

M. KITAGAWA
Department of Mechanical Engineering, Faculty of Technology, Kanazawa University, Kanazawa, Japan

The general process of fracture in notched polycarbonate, poly(vinyl chloride) and poly(methyl methacrylate) bars subjected to three-point bending has been investigated at various temperatures. Fracture nuclei initiate at the tip of the plastic deformation zone which resembles the slip-line field for yielding from a circular hole, and propagate to form a final fracture. A slip-line field analysis, which takes into account the effect of the hydrostatic stress component on the yield criterion, is executed to determine the stress components in the plastic zone and a criterion on the initiation of the fracture nucleus is discussed.

1. Introduction

Plastic deformation and fracture processes in glassy polymers have been investigated in recent years. Argon and co-workers [1] indicated that when the specimen contained discontinuities such as notches or was homogeneously stressed by a flat punch, the inhomogeneous plastic strain occurred in the form of intense shear bands. These bands have been studied by many workers, notably Bowden and Raha [2], and Brady and Yeh [3]. From studying many electron fractographies Chau and Li [4, 5] suggested that micro-cracks were occasionally generated at the intersections of the shear bands. Murray and Hull [6] and Doyle *et al.* [7] investigated the brittle fracture process using smooth specimens of amorphous glassy polystyrene and revealed several striking features not found in other materials such as metals and their alloys. Based on the examination of the surface morphology of broken specimen, they showed that in polystyrene, as in most glassy polymers, fracture started with the formation of a craze sheet, was followed by the nucleation and slow growth of a crack, and was completed by rapid crack propagation. Less attention has been paid to the mechanism of the notch brittle fracture, especially in relation to the formation of deformation bands.

Grade and Weiss [8], and subsequently Mills [9] and Narisawa *et al.* [10] showed that a flaw, which is not definitely identified as a craze or crack, formed at the elastic–plastic boundary below the notch and led to fracture in slow tensile, impact bending and three-point bending tests of edge-notched polycarbonate sheets. According to the results, the fracture process passes through three stages as follows: (1) initiation and growth of shear deformation bands; (2) nucleation and slow growth of a crack-like flaw below the notch; and (3) rapid propagation of the flaw. These observations are very similar to the notch cleavage fracture of steel at low temperatures. Knott and Cottrell [11] were the first to note this mechanism. According to their slip-line field analysis, the normal stress to open and spread a crack, highest at the elastic–plastic boundary due to plastic constraint, was recognized to be nearly constant over the cleavage fracture temperature ranges. Thus, they proposed a critical normal stress criterion on the cleavage fracture. The subsequent experimental results showed that this criterion was successfully applied to account for the notch brittle fracture [12, 13].

Following this suggestion, Mills [9] and Narisawa *et al.* [10] calculated the stress components required for flaw initiation in polycar-

0022–2461/82/092514–11$03.82/0

bonate samples on the basis of the slip-line field theory for a rigid, perfectly plastic material, and the results were compared with Argon's criterion for craze nucleation [14]. However, since in general the yield criterion of polymers is pressure dependent, the slip-line field analysis used for a pressure independent yield material tends to over estimate the stress components around the notch, as described later. Furthermore, this kind of flaw initiation in glassy polymers does not seem to be fully understood due to the lack of experimental results.

The purpose of this paper therefore, is, to provide more experimental evidence of the mechanism of fracture in glassy polymers and to describe a criterion for flaw initiation. Then specimens with various notch root radii machined from three kinds of glassy polymers are prepared and subjected to three-point bending.

2. Slip-line field around a circular notch

It has been well established that the yield condition of glassy polymers is influenced by the first invariant of the stress tensor, and several criteria on the yielding have been proposed. One of the useful equations is a pressure-dependent von Mises yield criterion of the form [15]

$$\alpha J_1 + J_2^{1/2} = k, \tag{1}$$

where J_1 and J_2 are the first and the second stress invariants of the stress tensor, respectively, k is the shear yield stress at a pure shear state where there is no dilatational stress and α is the positive material constant. In Cartesian co-ordinates x, y, and z, J_1 *and* J_2 are described by

$$J_1 = \sigma_x + \sigma_y + \sigma_z$$

$$J_2 = \tfrac{1}{6}\left[(\sigma_x - \sigma_y)^2 + (\sigma_y - \sigma_z)^2 + (\sigma_z - \sigma_x)^2\right] + \tau_{xy}^2 + \tau_{yz}^2 + \tau_{zx}^2 .$$

When $\alpha = 0$, Equation 1 reduces to the well-known von Mises criterion.

In the plane strain deformation of a rigid, perfectly plastic material when there is no strain in the z direction, σ_z is obtained from Equation 1 as

$$\sigma_z = \tfrac{1}{2}(\sigma_x + \sigma_y) - 3\alpha J_2^{1/2}$$

and, therefore, Equation 1 rewritten as

$$\left[\left(\frac{\sigma_x - \sigma_y}{2}\right)^2 + \tau_{xy}^2\right]^{1/2} + \frac{\sigma_x + \sigma_y}{2} - c\cos\phi = 0, \tag{2}$$

where $\sin\phi = 3\alpha/\sqrt{(1 - 3\alpha^2)}$ and $c\cos\phi = k/\sqrt{(1 - 3\alpha^2)}$. The stress components at any points in the field are described by

$$\sigma_x = p(1 + \sin\phi\cos 2\eta) + c\cos\phi$$

$$\sigma_y = p(1 - \sin\phi\cos 2\eta) + c\cos\phi$$

$$\tau_{xy} = p\sin\phi\sin 2\eta, \quad p = (\sigma_1 - \sigma_2)/2\sin\phi$$

where σ_1 and σ_2 are the minimum and the maximum principal stresses, respectively, and η is the anticlockwise angle between the x axis and the σ_1 direction [16].

From the equations of stress equilibrium in plane strain and Equation 3, we can obtain the characteristic lines and the differencial equations along them as follows

$$\frac{dy}{dx} = \tan\left[\eta \pm \left(\frac{\pi}{4} - \frac{\phi}{2}\right)\right] \tag{4}$$

$$dp \pm 2p\tan\phi\, d\eta = 0, \tag{5}$$

where the upper and lower signs correspond to α and β lines, respectively. Integrating Equation 5 along α or β line leads to Hencky's equations for a pressure-dependent yield material

$$p\exp(2\eta\tan\phi) = C_\alpha$$

$$p\exp(-2\eta\tan\phi) = C_\beta, \tag{6}$$

where C_α and C_β are the constants.

A slip-line field solution for a round notched bar of a pressure-dependent yield material is slightly different from the well-known one given by Hill. For a plane strain tension, the slip lines derived from Equation 4 are a kind of logarithmic spirals described by

$$r/\rho = \exp\left[\pm\theta\cot\left(\frac{\pi}{4} - \frac{\phi}{2}\right)\right], \tag{7}$$

where the upper and lower signs correspond to α and β lines, respectively, r and θ are the polar co-ordinates and ρ is the notch root radius. The stresses for polar co-ordinates are given by

$$\sigma_{\theta\theta} = \left[1 - \frac{1 - \sin\phi}{1 + \sin\phi}\left(\frac{r}{\rho}\right)^{-\frac{2\sin\phi}{1+\sin\phi}}\right] c\cot\phi$$

$$\sigma_{rr} = \left[1 - \left(\frac{r}{\rho}\right)^{-\frac{2\sin\phi}{1+\sin\phi}}\right] c\cot\phi$$

$$\sigma_{r\theta} = 0$$

$$\sigma_m = \tfrac{1}{3}(\sigma_{rr} + \sigma_{\theta\theta} + \sigma_z)$$
$$= \left[1 - \frac{1 + \frac{1}{3}\sin^2\phi}{1 + \sin\phi}\left(\frac{r}{\rho}\right)^{-\frac{2\sin\phi}{1+\sin\phi}}\right] c\cot\phi$$

where σ_m is the hydrostatic stress component. For a plane strain compression, ϕ should be replaced by $-\phi$ in Equations 7 and 8. In the case of $\Phi = 0$, Equations 7 and 8 reduce to the well-known solutions. α and β lines, in general, do not intersect at 90°. The acute angle of the intersection, which becomes equal to 90-ϕ°, decreases with an increase in a parameter ϕ. Figure 1 shows Equation 7 with three values of ϕ. The experimental curves dicussed later are also indicated in the figure.

Figure 2 shows the variation of $\sigma_{\theta\theta}/2k$ with r/ρ for several values of ϕ. It should be noted here that k is the shear yield stress tested in the absence of dilatational stress. The maximum principal stress is found to be greatly affected by ϕ. As the value of ϕ increases, the rate of change in $\sigma_{\theta\theta}/2k$ with r/ρ decreases and the maximum stress decreases considerably. Hence, it is found that the stresses estimated from the slip-line field for a rigid, perfectly plastic material involve a large error. As described later, the intersection angle for the materials tested here is about 80°, i.e., $\phi = 10°$. In this case, the maximum stress $\sigma_{\theta\theta}$ becomes 0.2 to 0.3 times smaller than the solution of $\phi = 0°$.

If the thickness of the notched bar is thicker than the region of logarithmic spirals, the maximum stress is described by

$$\sigma_{\theta\theta} = \left\{1 - \frac{1-\sin\phi}{1+\sin\phi} \times \exp\left[-2\left(\frac{\pi}{2} - \omega\right)\tan\phi\right]\right\} \times c\cot\phi, \quad (9)$$

where ω is the half angle of the notch.

In the case of pure bending of unnotched specimen, a yield moment M_y per unit width is given by

$$M_y = \tfrac{1}{2} c \cos\phi a^2, \quad (10)$$

where a is the thickness of specimen.

Although these solutions are successfully applied to metals, these may not be completely valid for soft materials like polymers with relatively low elastic modulus. However in the present paper, for simplicity, we use these equations for estimating the stress components around the notch.

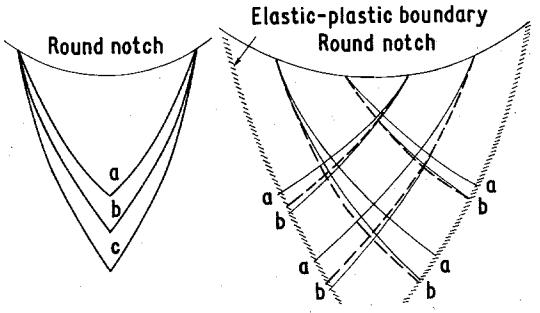

Figure 1 Comparison between experimental and theoretical slip lines. The solid lines, a, b and c are derived from Equation with $\phi = 0°$, 10° and 20°, respectively. The broken lines are experimental.

3. Experimental procedure

The materials used were commercial polycarbonate (PC), poly(vinyl chloride) (PVC) and poly(methyl methacrylate) (PMMA) plates 10 mm thick (Takiron Co., Japan). Test pieces with various dimensions of round notch were machined from these plates. All specimens were then annealed for two hours slightly above the glass transition temperatures and slowly cooled down to room temperature in an electric oven. The shapes and dimensions of test pieces are shown in Fig. 3.

Three-point bending tests were executed at a constant cross-head speed of 0.7 mm min^{-1} at temperatures of −20 to 80° C. The schematic illustration is shown in Fig. 3. The temperature

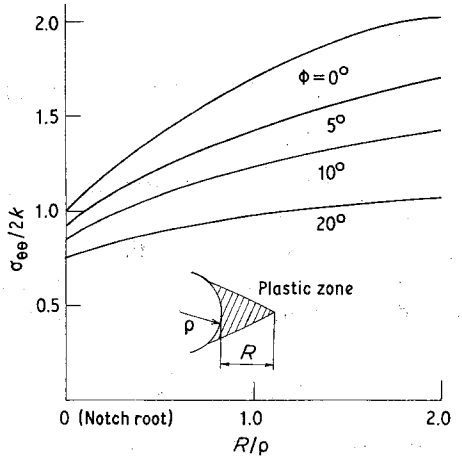

Figure 2 Theoretical (Equation 8) variation of $\sigma_{\theta\theta}/2k$ with R/ρ ahead of a notch at a given value of plastic zone size R for several values of ϕ.

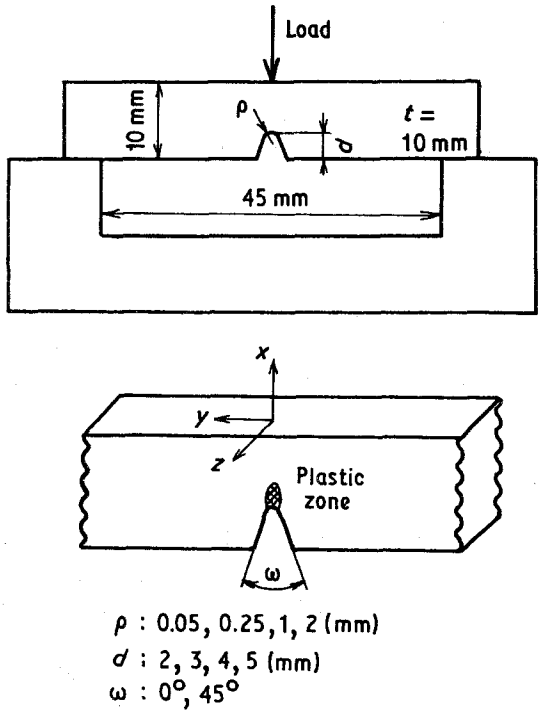

Figure 3 Schematic illustration of three-point bending test and specimen dimension.

variation measured by a copper–constantan thermocouple was within ± 0.5° C during the test. Load–displacement curves were traced on an X–Y recorder.

Microscopic observations were made on the specimen unloaded during deformation and after fracture. Thin slices were cut parallel (x–z plane in Fig. 3) and normal (x–y plane) to the notch plane to observe the plastic zone extension from the notch tip and the nucleus of fracture. Plastically deformed sections parallel to the x–z plane were metallographically polished, and the surface relief produced by the back deformation of shear bands upon raising the temperature to the glass transition temperature was observed through an optical microscope in order to investigate the difference between the plastic zone shape at the surface (plane stress) and that at the mid-thickness (plane strain).

4. Results

4.1. Temperature dependence of fracture load

The effect of temperature on fracture or general-yield load is shown in Figs 4, 5 and 6. The curves are similar for all three materials used. In the temperature ranges tested, the fracture load

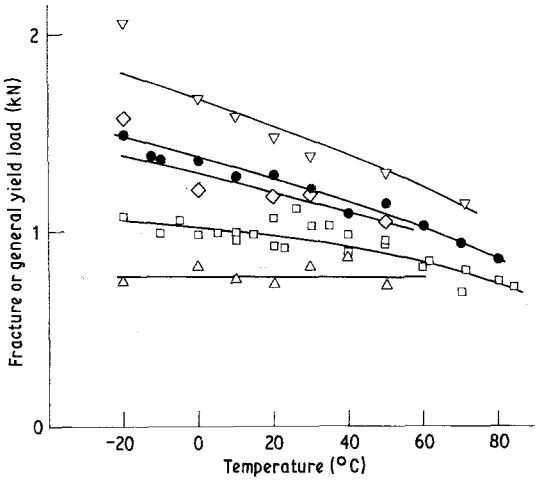

Figure 4 Effect of temperature on fracture or general yield load for various notch radii in PC ($d = 2$ mm, $\omega = 45°$). △ $\rho = 0$; □ $\rho = 0.25$, ◇ $\rho = 1$; $\rho = 2$; and ○ unnotched. The open and solid marks correspond to fracture and general yielding, respectively.

increases with decreasing temperature and increasing notch radius. At a certain temperature, depending on the radius of notch, there is a sharp change from fracture to general yielding. Above this temperature, the general yielding occurs before fracture. The plastic constraint factor, i.e., the ratio of the general yield load of notched specimen to that of unnotched specimen, is about 1.14 for the specimen with $\rho =$ 0.25 mm, the value of which is nearly equal to the result of Green [17].

The observations by unaided eye show that a disk-shaped region (fracture nucleus) is nucleated at a small distance from the notch root, grows

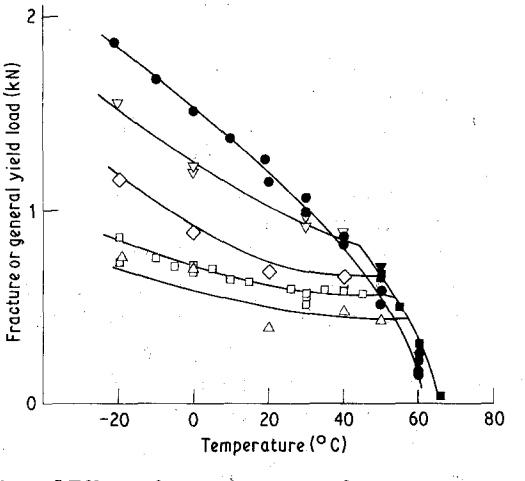

Figure 5 Effect of temperature on fracture or general yield load in PVC. The symbols are the same as Fig. 4.

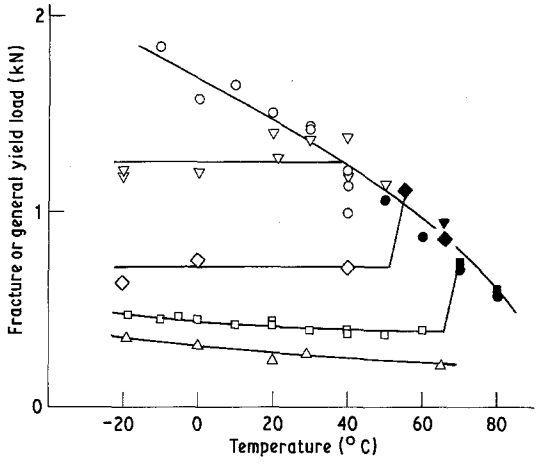

Figure 6 Effect of temperature on fracture or general yield load in PMMA. The symbols are the same as Fig. 4.

slowly and suddenly propagates to lead to a final fracture. The load at which the fracture nucleus initiates is slightly smaller than the fracture load. As the notch radius becomes small, the discrepancy between the fracture and nucleus initiation loads becomes large. But the nucleus initiation load against temperature curves are very similar to the results of Figs 4, 5 and 6.

4.2. Plastic zone extension

The patterns of the mid-section plastic zones for the specimen with $\rho = 2\,\text{mm}$ and $d = 2\,\text{mm}$ in PC are shown in Fig. 7. Similar observations were made of the polymers used here. The deformation zones of PVC samples, which appeared like white clouds, were too vague to be observed through an optical mircoscope. Their patterns seemed to be similar to those of PC by unaided eye. On the other hand, for PMMA, fracture occurred in a brittle manner without visible deformation zones. In this section, therefore, the results of PC are discussed.

The deformation zones, which consist of numerous fine bands, are first observed for $P/P_y = 0.65$ in a specimen with $\rho = 2\,\text{mm}$, where P is the applied load and P_y is the general yield load of the unnotched specimen. The deformation zones were shaped like small triangular wedges at the notch root. As the plastic zone is enlarged by further loading, the sides of the triangle become curved and a kind of logarithmic spiral becomes evident. When P/P_y reaches about 1.2, the fracture nucleus, the details of which are discussed later, initiates and a small increase in the applied load causes its growth. In the case where fracture does not occur, the state of general yield is achieved as shown in Fig. 7d. When the applied load is sufficient to cause general yielding, plastic hinges form at the mid-thickness and grow across the specimen. This pattern at the general yield state is similar to the theroetical slip-line field of Green and Hundy [18].

The experimental ratios of the plastic zone size R to the notch radius ρ, R/ρ, are plotted against P/P_y for specimens with varying root radii in Fig. 8. An increase in P/P_y causes R/ρ to increase, which, in turn, causes the maximum stress at the elastic–plastic interface to increase up to a critical value required for the information of the fracture nucleus.

Comparison of the experimental deformation bands with the theoretical logarithmic spirals is shown in Fig. 1. The experimental α and β lines do not intersect at 90°. The acute angle of intersection is about 80°, i.e. $\phi = 10°$. This value coincides with the intersection angle of two slip bands measured in the tensile part of an unnotched sample subjected to three-point bending. The experimental curves seem to be slightly different from the theoretical ones derived from Equation 7 with $\phi = 0°$ and 20°. On the other hand, the theoretical slip lines (b in Fig. 1) with $\phi = 10°$ are in good agreement with the experimental results. This agreement may be due in part to the fact that the specimen is not thick enough to be in a complete plane strain state over its thickness, but may arise mainly because the polymer yield criterion is pressure dependent.

The depth of penetration of the plastic zone was measured at various positions along the notch root to estimate the degree of plane strain. The samples cut parallel (x–z plane) to the notch plane were polished, annealed slightly above the glass transition temperature, and were observed through an optical microscope. The results are presented in Fig. 9. In the neighbourhood of the specimen surface, deformation bands propagate in the x direction, but at the mid-section, they grow parallel to the notch root (z direction). The change from hinge (plane stress) to wedge (plane strain) plastic patterns is found to occur with increasing width. The penetration depth of the plastic zone is not very different between the surface and the mid-section. From that it is inferred that true plastic strain would be achieved at the centre of a specimen about 5 mm wide.

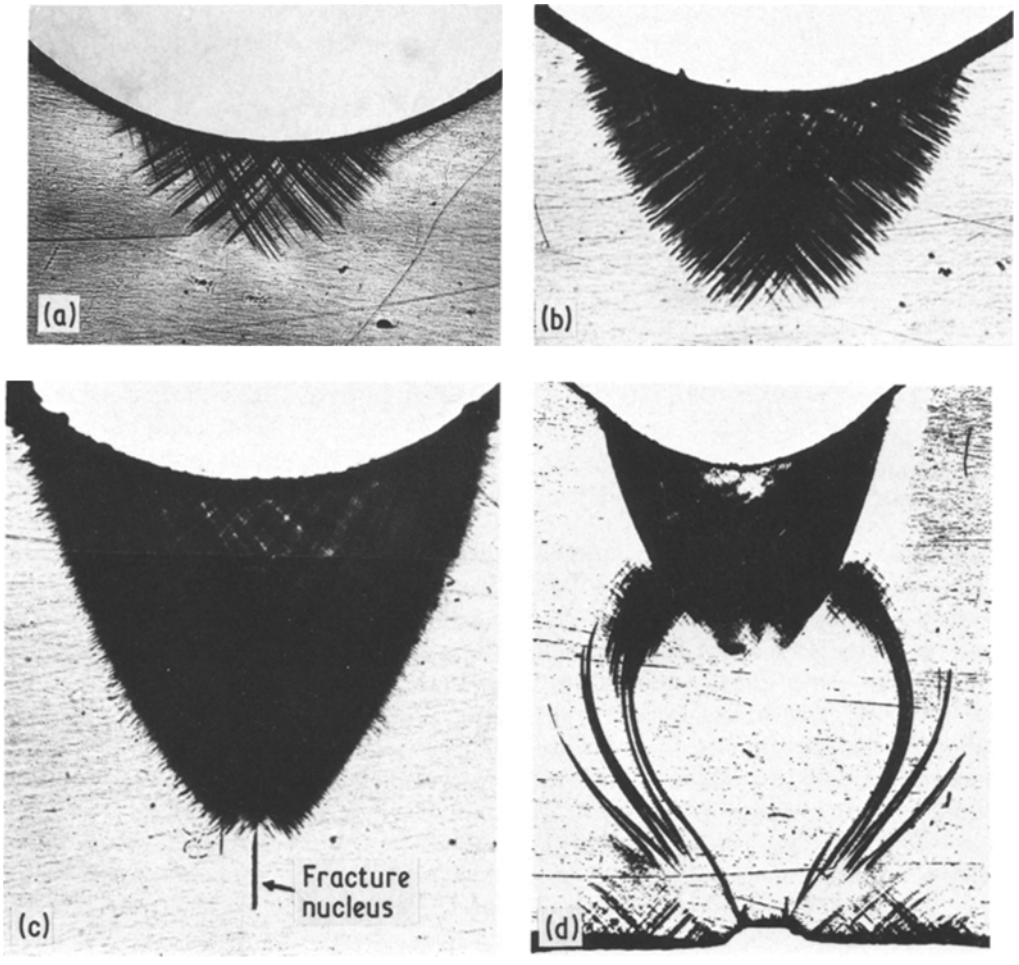

Figure 7 Plastic zone extension from a round notch of $\rho = 2$ mm. (a) $P/P_y = 0.81$; (b) $P/P_y = 1.05$; (c) $P/P_y = 1.23$; and (d) at general yielding ($d = 5$ mm).

4.3. Initiation of a fracture nucleus and fracture surface

When the applied load increases and reaches a critical value dependent on the notch dimension, internal disks nucleate near the tip of the plastic deformation zone as shown in Fig. 7c. These disks were observed as a series of concentric interference fringes by an optical microscope as indicated by Mills [9] and Narisawa *et al.* [10]. When annealed above the glass transition temperatures, the disks observed for both PC and PVC disappeared. These facts may indicate that the disk is a craze, and not a crack, as pointed out by Mills [9]. However, since the disc is not definitely confirmed as a craze, we shall call it the fracture nucleus.

For PC, the number of sites at which the fracture nuclei initiated was small and their positions were limited to the vicinity of the elastic–plastic interface, apart from the notch root. On the contrary, for PVC, many nuclei, which were small in size, formed all over the plastic deformation region, and one of them, near the tip of the plastic zone, propagated and led to fracture. This was not true for PMMA, where fracture occurred at the notch root without visible slip bands. This may be because the stress at the notch root arises due to the elastic stress concentration, reaches a critical value required for crack initiation before deformation bands grow inward, and thus fracture occurs in an elastic state.

Figure 10 represents an enlargement of the fracture nucleus shown in Fig. 7c. The intersection of the deformation bands with the plane of the nucleus is evident. The slip bands jump

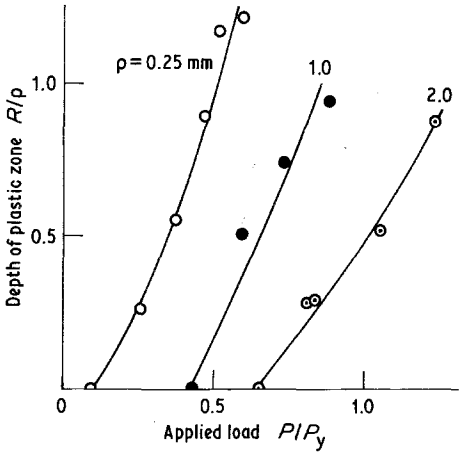

Figure 8 Experimental relationship between plastic zone size and applied load for various notch root radii in PC.

into the nucleus to form the so-called intrusion or extrusion which is occasionally observed in the early stage of fatigue of metals. This photograph gives the impression that the intersection of two (α and β) slip bands cause a wedge-shaped flaw. This mechanism, which is equivalent to the Cottrell model of brittle fracture of crystalline solids, is successfully used to explain the experimental results of craze initiation at a biaxial stress state under the action of a crazing agent [19]. Whether this is a suitable model for polymer fracture or not should be judged from experimental observations in the future.

These nuclei were observed not only for notched specimens, but also for unnotched specimens in PVC. They initiated at the mid-section of unnotched specimens and became the origin of a final fracture. In this case, the plastic zone was shaped like a triangle, but not like a logarithmic spiral. According to the slip-line field theory described above, the stress state over the triangular zone is uniform and the stress state at the position at which the nuclei are generated becomes equal to that at the lower surface subjected to tensile stress. Why do the nuclei initiate at the mid-section, but not at the surface? The nucleus is accompanied by the shear bands for both PC and PVC.

Figure 11 shows an example of the micrographs of the fracture nucleus in PC. The process mentioned above is reflected in the photograph. The nucleus A, which exists at a short distance from the notch root, grows elliptically from the spot-like origin 0 adjacent to the deformation bands B2 observed as irregular lines. The nucleus spreads slowly in both x and z directions (Fig. 3) at the same time. The growth rate is high in the z direction than in the x direction and thus it becomes elliptical. Outside the region A, the crack generated within the nucleus becomes unstable. The comparatively flat region B1 involves typical brittle features such as mackerel and rib marks. The rough region B2 forms when the crack propagates towards the notch root through the plastic zone and encounters the shear bands which act as an obstacle to its growth. If the shear bands are intense enough to prevent the crack propagation, the crack grows in a shear mode along one of the shear bands, and the fracture surface is very different from the regions, A, B1 and B2 as shown in Fig. 12. From these photographs, it is found that the shear bands play an important role in the formation of the fracture nucleus and its growth.

Similar results are obtained for PVC except for the non-existence of the region B2. The shear bands are not as intense as mentioned in the previous section, and the nucleus grows towards and reaches the notch root, before a brittle crack initiates.

In contrast to the results of both PC and PVC, most nuclei in PMMA initiate at the notch root and are rarely away from the notch root. The fracture surface consisting of the slow and rapid crack growth regions becomes relatively smooth and featureless.

5. Discussion

The nucleus initiation load is slightly smaller than the fracture load. In PC, the ratios of that load P_c to the general yield load of unnotched samples P_y were about 0.55, 0.8 and 1.2 for specimens with $\rho = 0.25$, 1 and 2 mm, respectively. These values were not so temperature-dependent. For PVC, P_c could not be determined distinctly because of the vagueness of the nucleus initiation.

Measurements were made of the distance of the nucleus position from the notch root R_F on broken samples with various notch dimensions through an optical microscope. In the case of $\rho = 0$, fracture occurred very near or at the notch root and R_F could not be determined. The results are shown in Fig. 13. The measured values of R_F/ρ are nearly coincident with the values expected from Fig. 8 and the measured values of P_c/P_y. Except for the data of $\rho = 0.25$ mm, the values of R_F/ρ are about 0.8 for PC and 0.3 for PVC. For a PC specimen with $\rho = 0.25$ mm, its value

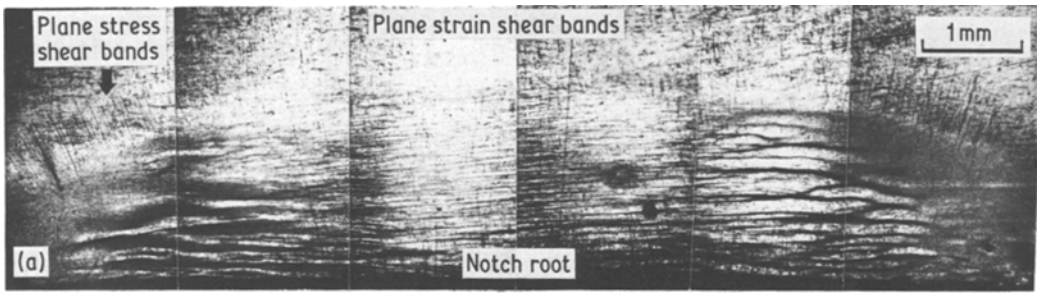

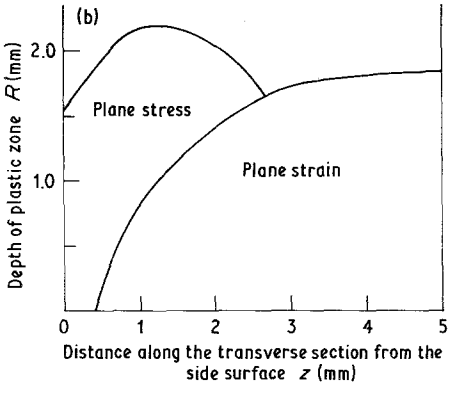

Figure 9 Variation of plastic zone size across the thickness (z) direction for a PC specimen with $\rho = 2$ mm and $d = 2$ mm. (a) Shear bands produced by the back deformation upon raising the temperature to the glass transition temperature. (b) Diagram showing the degree of plane strain.

is about 1.15, which is considerably higher than the above-mentioned value.

By applying the slip-line field theory to the results of Fig. 13, the maximum principal stress σ_F and the hydrostatic stress component σ_{mF} for the nucleus initiation can be estimated. Detailed observations of the angle at which two (α and β) slip lines intersect each other were made for both notched and unnotched specimens. The results of both PC and PVC indicated that the acute angle of the slip-band intersection was about 80°, i.e., $\phi = 10°$ and was almost insensitive to temperature. Then, ϕ is set equal to 10° for both polymers. For PVC, $\sigma_F/2k$ and $\sigma_{mF}/2k$ are estimated from Equation as about 1.0 and 0.56 respectively in the temperature ranges lower than 30° C. Above this temperature, these values increase steeply. For PC, in the case of $\rho =$ 0.25 mm, $\sigma_F/2k$ and $\sigma_{mF}/2k$ are obtained as 1.25 and 0.91. When $\rho = 1$ and 2 mm, $\sigma_F/2k = 1.18$ and $\sigma_{mF}/2k = 0.8$. In contrast to the result of PVC, these values are dependent on the notch radius. This may indicate that σ_F and σ_{mF} increase as ρ decreases. The probable primary reason for this result is a steep stress gradient at the notch

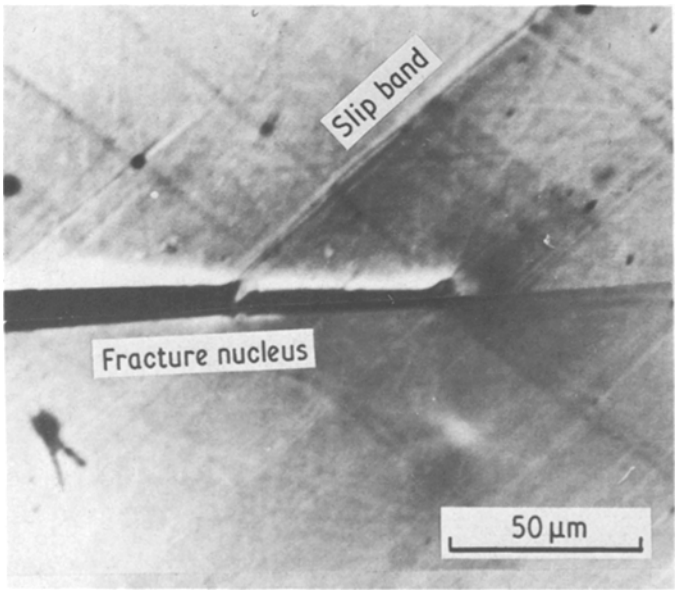

Figure 10 Enlargement of the fracture nucleus shown in Fig. 7c.

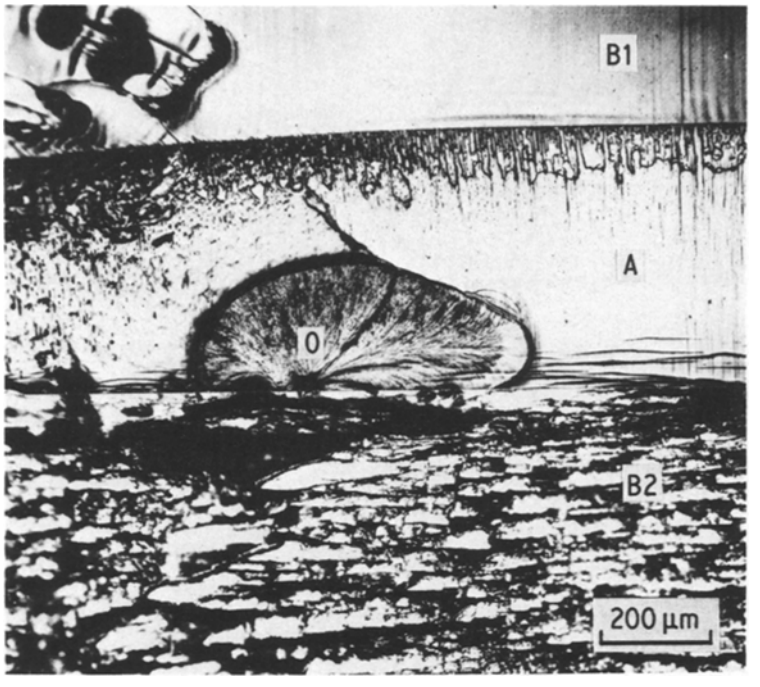

Figure 11 Typical example of fracture surface near the fracture origin in PC.

tip, as described by Tetelman *et al.* on the notch brittle fracture of steel [20]. This may be an apparent effect that occurs because σ_F at the elastic–plastic boundary must equal a critical value σ_F^* over at least an effective distance t_e to allow fracture nucleation. For example, when $\sigma_{\theta\theta} = \sigma_F^*$ at the elastic–plastic boundary (Fig. 14a), fracture nucleus initiation cannot occur because the sharp stress gradient causes $\sigma_{\theta\theta}$ to be less than σ_F^* over the effective distance t_e. The fracture nucleus will form if $\sigma_{\theta\theta} \geqq \sigma_F^*$ over t_e. According to the diagram shown in Fig. 14b, the plastic zone must spread over the distance $(t_e + R_0)$ (R_0 being defined in Fig. 14). This

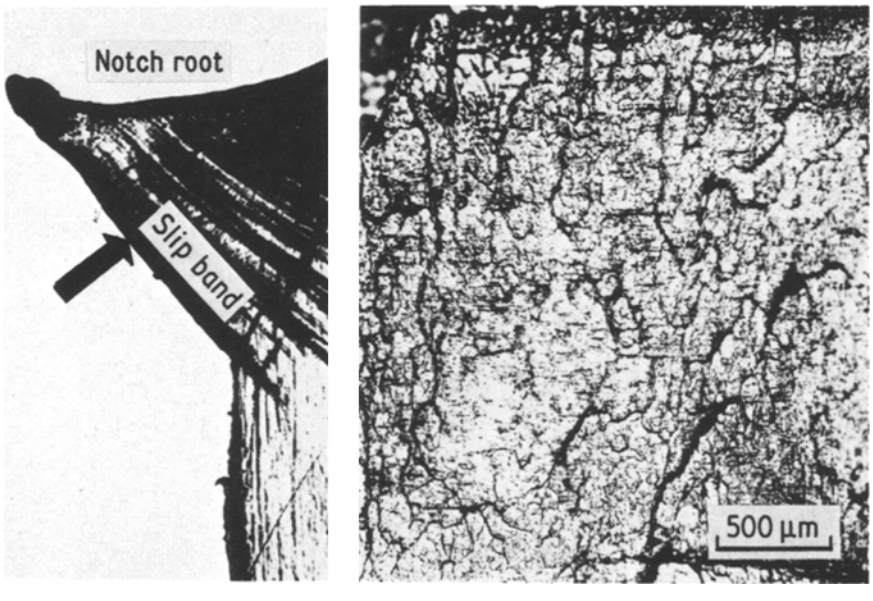

Figure 12 Shear fracture along intense slip band and its surface. The arrow shows the direction from which the fractograph was taken.

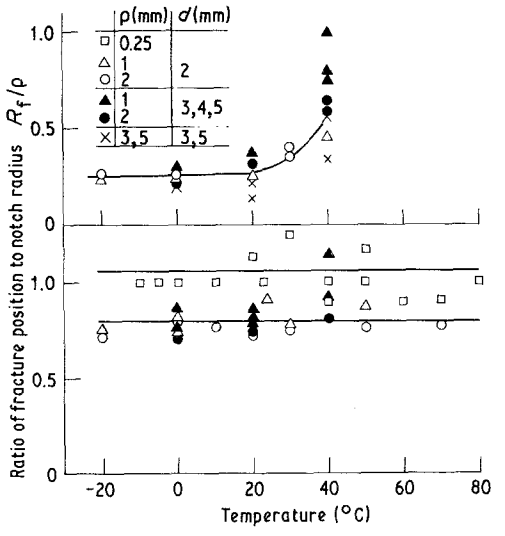

Figure 13 Experimental variation of fracture position with temperature in PC and PVC.

model was successfully applied to notch brittle fracture of steel. If the effective distance t_e is assumed to be about 0.09 mm in PC, σ_F^* becomes equal to $2.4k$.

The pure shear yield stress k is calculated by the experimental results of Figs 4 to 6 and the equation

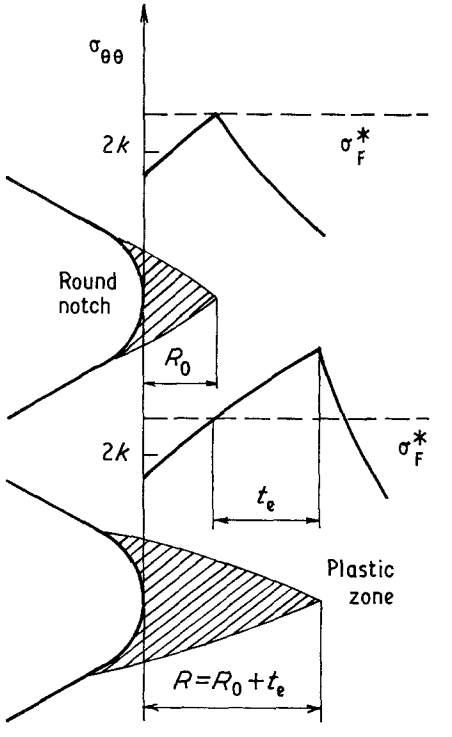

Figure 14 Effect of a steep stress gradient on the criterion for the initiation of a fracture nucleus.

$$M_y = \frac{P_y l}{4} = \tfrac{1}{2} c \cos\phi a^2 b$$

$$= \tfrac{1}{2}\sqrt{1 + \tfrac{1}{3}\sin^2\phi}\, ka^2 b$$

where l is the span length, b the specimen width and P_y the general yield load of unnotched specimen, As shown in Figs 4 to 6, P_y, and therefore k, are temperature dependent. Thus the critical stress σ_F^* increases with decreasing temperature. This is different from the result for steel [21]. For example, in PC, σ_F^* is estimated as about 90 MPa at 50° C, 105 MPa at 20° C and 125 MPa at − 20° C.

Suppose that the fracture nucleus is a craze. The maximum principal stress for craze initiation is found not to vary with the first stress-invariant σ_m in a stress state where σ_m is dilatational [22], and hence the criterion may be recognized to obey the maximum principal stress. For this reason, σ_F^* may becomes constant irrespective of the notch dimension.

6. Conclusion

The notch brittle fracture of glassy polymers was investigated in connection with the shear band growth and the subsequent initiation of fracture nucleus in the temperature ranges − 20° to 80° C. Below a temperature above which general yielding occurs, a crack-like flaw (fracture nucleus) is generated at the elastic–plastic interface and causes a brittle fracture in PC and PVC, while PMMA fractures in an almost elastic state.

The shape of the shear bands formed around the notch root coincides with a pair of characteristic lines derived from the slip-line field theory, taking into account the effect of the first stress invariant on the yield criterion. The critical tensile stress for the nucleus initiation was calculated from the slip-line field theory for a pressure-dependent yield material. The critical stress averaged over an effective distance at the position of fracture nucleus appears to be independent of the notch dimension. However, its value varies with temperature. For nucleus initiation under a stress state where the hydrostatic stress component is dilatational, the maximum principal stress theory may be applicable.

Acknowledgement

I am grateful to Mr F. Taniguchi and Mr A. Fukami for their technical assistance.

References

1. A. S. ARGON, R. D. ANDREWS, J. A. GODRICK and N. WHITNEY, *J. Appl. Phys.* **39** (1968) 1899.
2. P. B. BOWDEN and S. RAHA, *Phil. Mag.* **22** (1970) 463.
3. T. E. BRADY and G. S. YEH, *J. Appl. Phys.* **42** (1971) 4622.
4. C. C. CHAU and J. C. M. L. LI, *J. Mater. Sci.* **14** (1979) 1593.
5. *Idem, ibid.* **14** (1979) 2172.
6. J. MURRAY and D. HULL, *J. Polymer. Sci A-2* **8** (1970) 583.
7. M. J. DOYLE, A. MARANCI, E. OROWAN and S. T. STORK, *Proc. Roy. Soc. London* **A329** (1972) 137.
8. A. M. GRADE and V. WEISS, *Met. Trans.* **3** (1971) 2811.
9. N. J. MILLS, *J. Mater. Sci.* **11** (1976) 363.
10. N. ISHIKAWA, I. NARISAWA and H. OGAWA, *J. Polymer. Sci. A-2* **15** (1977) 1791.
11. J. F. KNOTT and A. H. COTTRELL, *J. Iron Steel Inst.* **201** (1963) 249.
12. T. R. WILSHAW and P. L. PRATT, *J. Mech. Phys. Solids* **14** (1966) 7.
13. G. D. FERNEBOROUGH and C. J. HOY, *J. Iron Steel Inst.* **202** (1964) 912.
14. A. S. ARGON, *Pure Appl. Chem.* **43** (1975) 247.
15. P. B. BOWDEN and J. A. JUKES, *J. Mater. Sci.* **7** (1972) 52.
16. A. MAKINOUCHI, *J. Japan Soc. Tech. Plasticity* **17** (1976) 140 (in Japanese).
17. A. P. GREEN, *Q. J. Mech. Appl. Meth.* **6** (1953) 223.
18. A. P. GREEN and B. B. HUNDY, *J. Mech. Phys. Solids* **4** (1956) 128.
19. M. KAWAGOE and M. KITAGAWA, *J. Polymer. Sci. A-2* **19** (1981) 1423.
20. T. R. WILSHAW, C. A. RAU and A. S. TETELMAN, *Int. J. Eng. Fract. Mech.* **1** (1968) 191.
21. J. F. KNOTT, *J. Iron Steel Inst.* **204** (1966) 1014.
22. S. S. STERNSTEIN and L. ONGCHIN, *Polymer Preprints Amer. Chem. Soc. Div. Polymer Chem.* **10** (1969) 1117.

Received 19 October 1981
and accepted 29 January 1982